SLAC-PUB--5595

DE91 015752

BEAMSTRAHLUNG SIMULATION AND DIAGNOSTICS*

V. ZIEMANN
Stanford Linear Accelerator Center
Stanford University, Stanford CA 94309

ABSTRACT

A simulation code that models the mutual deflection and the emission of beamstrahlung of two ultra-relativistic electron and positron bunches is described. The simulations are used to determine transverse beam sizes from observed beamstrahlung fluxes.

1. Introduction

At the interaction point of the SLC electron and positron bunches with energies of 46 GeV, transverse beam sizes of a few microns and a few times 10^{10} particles per bunch collide head on. The large number of particles in a small volume gives rise to large electromagnetic fields of up to 10 T which deflect the particles in the oppositely running bunch. The observed centroid deflection angles range up to 200 μrad and can be reconstructed from beam position monitor readings in the vicinity of the interaction point (IP). By deliberately sweeping one beam across the other with fast air-core magnets the deflection angle as a function of the relative distance of the two beams is recorded. The convoluted spot sizes $\Sigma = \sqrt{\sigma^2(e^-) + \sigma^2(e^+)}$ can then be calculated by fitting the well-known beam-beam deflection curve for round beams to the data [1].

As a complementary signal the synchrotron radiation flux from the beam-beam deflections, the so-called beamstrahlung, is recorded in two monitors about 40 m downstream of the IP. They are situated just after the first bending magnet that is used to separate particles and beamstrahlung, but generates synchrotron radiation itself. Owing to the large magnetic fields

Presented at the 7th ICFA Beam Dynamics Workshop,
Los Angeles, May 13-16, 1991

* Work supported by the Department of Energy, contract DE-AC03-76SF00515
† Presented at the 7th ICFA Beam Dynamics workshop, Los Angeles, May 13-16, 1991

in the beam-beam deflections the critical energies of the beamstrahlung is considerably higher than that of the synchrotron radiation from the bending magnet. The low energy photons are discriminated from the high energy beamstrahlung photons by the threshold effect of the monitor which first converts photons into e^+e^- pairs and then detects the Cerenkov light emitted by those pairs in a volume of ethylene gas at low pressure [2].

The widths of the beamstrahlung flux curves, plotted versus the relative distance of the two beams is predominantly determined by the transverse beam sizes of the electron and positron beams. From horizontal and vertical beam-beam scans we obtain 2 "flux versus distance" plots from the radiating positrons and 2 from the radiating electrons. From those plots 4 widths can be extracted. Assuming 2 upright particle beams, characterized by σ_x and σ_y, the 4 transverse extensions of the beams uniquely determine the widths of the 4 beamstrahlung scans. The method, originally proposed by W. Kozanecki and E. Gero [3,4] uses a simulation code to determine the beamstrahlung widths for various given beam sizes and then sets up a table that maps beam sizes to widths. Given measured widths the beam sizes can then be inferred by a table inversion which is performed in a χ^2-sense.

2. The Simulation

The spectral characteristics of synchrotron radiation is most efficiently described by its critical energy $\varepsilon_c = 3\hbar c\gamma^3/2\rho$ which depends on the bending radius ρ a radiating particle experiences. The local bending radius varies as a particle traverses the oncoming bunch of the opposite charge according to

$$\frac{1}{\rho(x,y,t)} = |\Theta(x,y)| \frac{1}{\sqrt{2\pi}\sigma_z/2} \exp\left[-\frac{(ct)^2}{2(\sigma_z/2)^2}\right] \qquad (1)$$

where the entire transverse dependence is buried in the integrated deflection angle $\Theta(x,y)$ which is proportional to the transverse electric field of the oncoming bunch. $\Theta(x,y)$ is given explicitly in terms of complex error functions in Ref. 5.

In order to determine the number of generated Cerenkov photons per unit time we have to integrate the number of beamstrahlung photons per unit time and unit energy, given by [6]

$$\frac{dN}{d\varepsilon\, dt}(\varepsilon, \varepsilon_c(\rho(t))) = \frac{1}{\sqrt{3}\pi} \frac{\alpha^2}{r_e mc} \frac{1}{\gamma^2} \int_{\varepsilon/\varepsilon_c}^{\infty} ds\, K_{5/3}(s) \qquad (2)$$

over energy, weighted by the pair production probability $\gamma \to e^+e^-$ in the converter plate and the efficiency of converting a e^+e^- pair into a Cerenkov photon. The relation among the different spectra and efficiencies is depicted in Fig. 1.

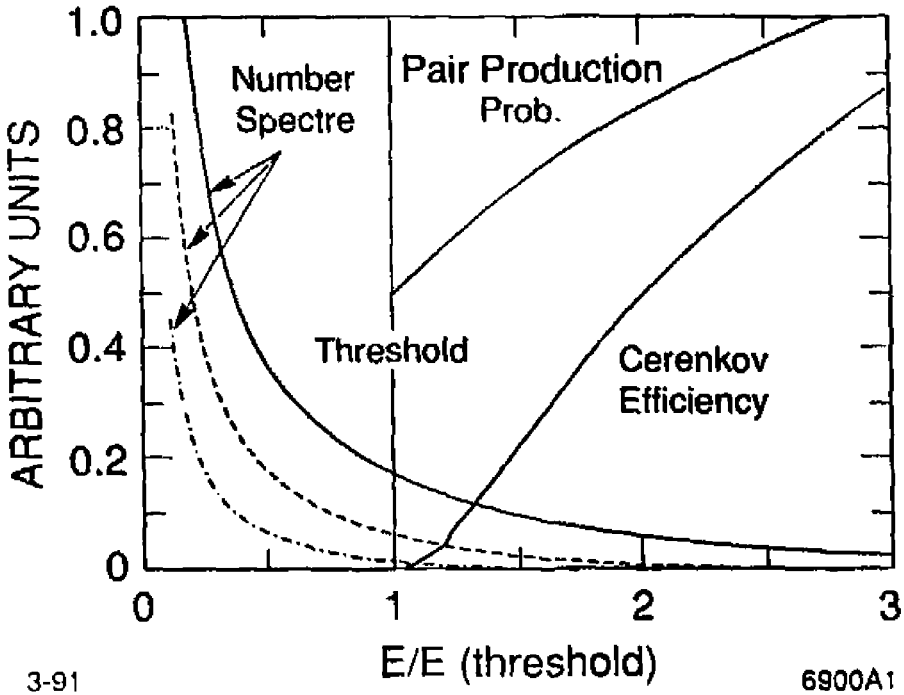

Figure 1: The pair production probability, Cerenkov photon generation efficiency and photon number spectra with critical energies of 1/2 (dotdashed),1 (dashed) and 2 times (solid) the Cerenkov threshold. The vertical bar at 1 *marks the Cerenkov threshold*

The resulting integral depends on two different energies: the critical energy and the threshold energy of the Cerenkov monitor. To a good approximation it can be shown [7] that the number of Cerenkov photons generated per unit time depends only on the ratio of the energies. The resulting calibration curve represents a transfer map that relates the local bending radius as experienced by the radiating particle to the number of Cerenkov photons per unit time.

The total number of Cerenkov photons generated in one beam traversal is given by the average over the path and the transverse distribution ψ_c of the radiating particles as given by

$$N \quad \int_{-\infty}^{\infty} dx \int_{-\infty}^{\infty} dy\, \psi_c(x,y) \int_{-\infty}^{\infty} dt\, \frac{dN_\gamma}{dt}(\rho(x,y,t)) \ . \qquad (3)$$

All dependence on the field producing distribution is buried in $\rho(x,y,t)$. In

order to eliminate one numerical integration we express $dN_\gamma/dt(\rho)$ in a power series and integrate term by term over t. The remaining integrals over x and y then have to be done numerically.

In the simulation code [8] this algorithm is used to calculate the Cerenkov fluxes as a function of the transverse distance of the two beams. In the next sections we will discuss how this can be used as a diagnostic tools to infer properties of the particle distributions, namely: which of the two beams is bigger and needs closer attention and by how much is it bigger.

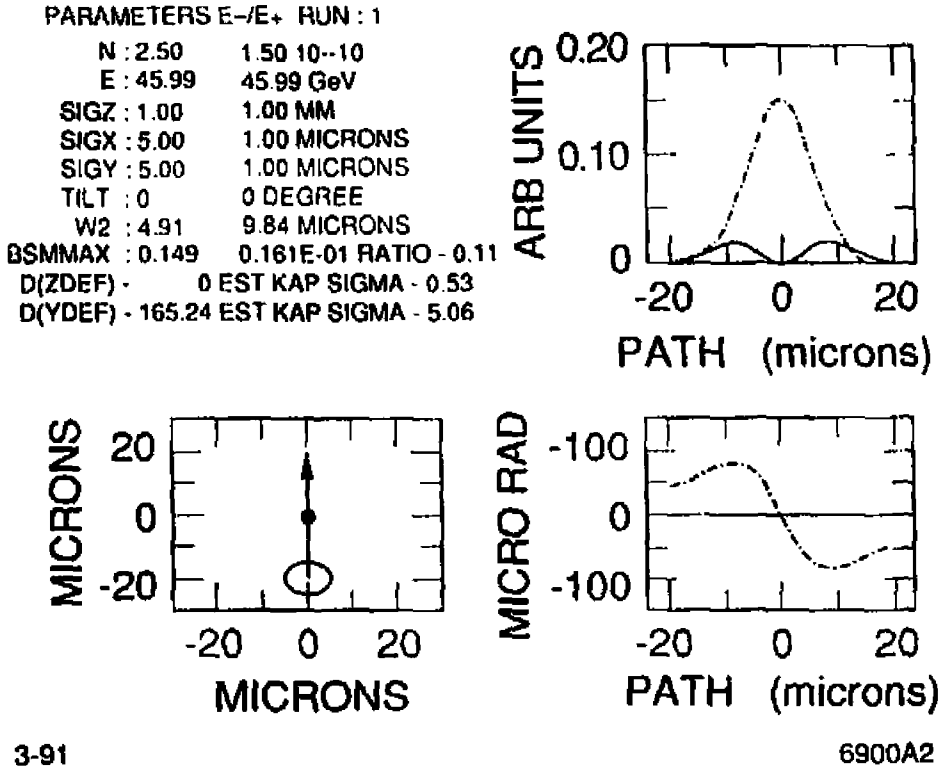

Figure 2: *A typical output from the simulation code. In the upper left the input data are echoed. In the upper right the beamstrahlung fluxes are shown in arbitrary units. The solid curve is the flux from the radiating positrons on the north monitor. In the lower left depicts the path on which the scan was taken and the lower right shows the electron deflection. Here the solid curve shows the horizontal deflection and the dashed curve the vertical.*

3. Simulation Results

Fig. 2 shows the result where a large electron beam with $\sigma_x = 5\,\mu m$ is passed over a small positron beam with $\sigma_x = 1\,\mu m$. The extrema of the beamstrahlung flux from the small e^+ beam (solid) coincide with the extrema of the deflection curve, because there the local bending radius the e^+ experience is largest. The deflection near the center of the target e^- beam is weaker and causes the dip. For an ideal point like e^+ source beam, the dip should decrease to zero.

The radiation from the electrons (dotdashed) reflects mainly the transverse distribution of the electron beam because only those e^- radiate that are intercepted by the fields of the positron beam which serves as a window to view the radiating electrons.

Simulations with varying bunch sizes of 3, 4, and $5\,\mu m$ for electrons and positrons confirmed the above observation [8] that *the dip is always associated with the larger target beam size*.

At first sight it appears obvious to associate asymmetric beamstrahlung scans with tilted beams. However, if the scan is centered, the beamstrahlung scans are still symmetric, because the configuration shortly before the source beam enters the target beam is (point) symmetric to that shortly after it exits. Therefore the fluxes are the same. In order to break this symmetry and examine the $x - y$ coupling we have to offset the beams with respect to each other. Fig. 3 shows the results where tilted beams are scanned with $3\,\mu m$ offset. Clearly now asymmetric scans are produced.

The fact that *tilted and offset beams produce asymmetric beamstrahlung scans* can be useful to diagnose tilted beams. However, only if the beams are known to be of equal size is it possible to determine the tilt direction of the individual beams [8].

The widths of the beamstrahlung scans show a weak dependence on the energy and the number of particles per bunch as well as on the bunch length of the beams [4]. The reason for this lies in the separation of transverse and longitudinal dependence exhibited in Eq. 1 which is largely preserved in the response of the Cerenkov monitor [7].

4. Spot Size Measurements

In order to follow the program outlined in the introduction the simulation code is run to set up a table that relates the 4 beam sizes $\sigma_x(e^-), \sigma_y(e^-), \sigma_x(e^+), \sigma_y(e^+)$ to the 4 produced beamstrahlung widths from horizontal and vertical scans emanating from electrons and positrons. The table is organized as follows

$$\sigma_x(e^-), \sigma_y(e^-), \sigma_x(e^+), \sigma_y(e^+) \rightarrow W_y(e^-), W_y(e^+), W_x(e^-), W_x(e^+)\ .$$

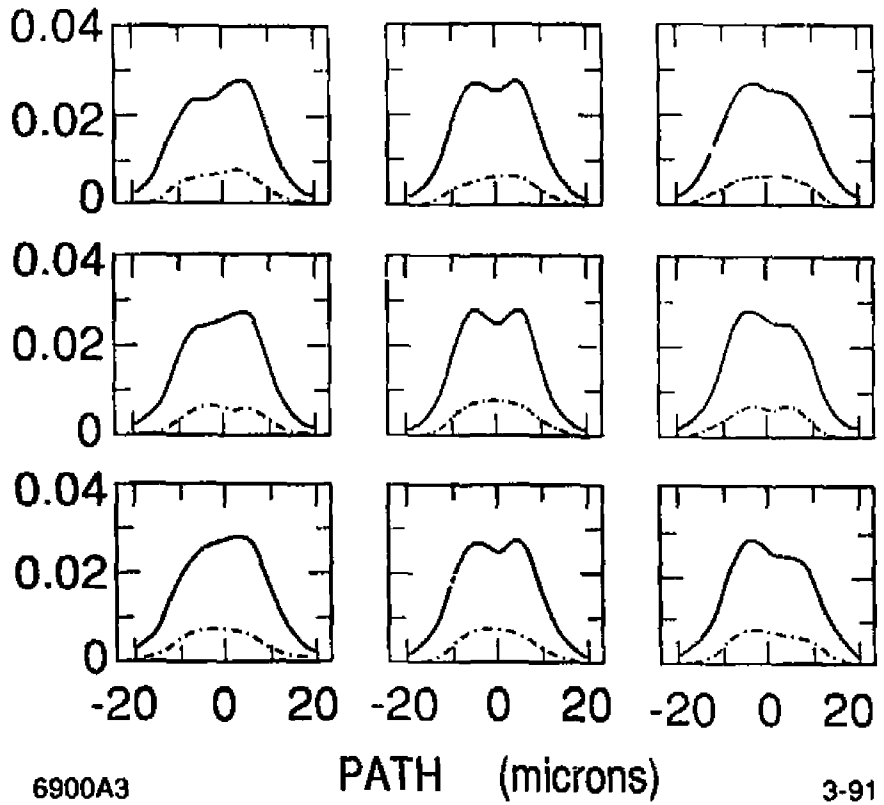

Figure 3: *Vertical beamstrahlung scans for tilted beams offset with respect to each other. The beam sizes for both beams are* $5 \times 3\,\mu m$. *The tilt angle is* -45, 0 *and* $+45$ *degree with respect to the horizontal axis from left to right for the positrons and top to bottom for electrons.*

Typically those tables contain 3^4 entries, because each of the 4 beam sizes assumes 3 different values, e.g. $1, 3, 5\,\mu m$.

The task of finding the beam sizes that produce a measured set of beamstrahlung widths is accomplished by inverting the table. This is done in a 3-step process. First, a "weighted table average" is calculated. In this pass a weight depending on the euclidean distance between the measured widths and the widths in the table is assigned to each table entry. Then the weight is used to average over the sigmas in the table. This process yields a rough estimate to start the second pass, which uses a linear interpolation on the table and a χ^2–minimization to zoom in on the beam sigmas that minimize the χ^2–difference between the measured widths and the interpolated table widths. In a third step an error estimate is performed by varying the

measured widths by a finite amount and observe how much the calculated beam sizes change.

It is planned to diagnose beam sizes using this method in the next SLC run and pursue the investigations undertaken earlier by W. Kozanecki and E. Gero.

5. Conclusion

A simulation code that calculates the beamstrahlung fluxes as a function of the relative distance of two ultra-relativistic beams was briefly described. The simulation results indicate that the *dip in the beamstrahlung scans can be attributed to a larger target beam size* and that *asymmetric scans are produced by tilted beams that are scanned with an offset*. Furthermore, a method to determine individual beam sizes from observable beamstrahlung widths was described. This method is based on construction of a table that relates beam sizes to widths. The "inversion" of this table can then be used to relate the widths to the beam sizes which produced them.

Acknowledgements

Discussions with E. Gero, C. Field and N. Toge are gratefully acknowledged.

References

1. W. Koska, et.al., SLAC-PUB-4919, 1989.
2. C. Field, NIM **A265**, 167, 1988.
3. W. Kozanecki, private communication
4. E. Gero, Ph.D. Thesis, Univ. of Michigan, 1991.
5. V. Ziemann, these proceedings and SLAC PUB 5582, 1991.
6. A. Sokolov, I. Ternov, *Synchrotron Radiation*, Pergamon Press, New York, 1968.
7. V. Ziemann, SLAC Collider Note CN-379, 1990.
8. V. Ziemann, SLAC Collider Note CN-381, 1990.